

Characterization of a monoclonal antibody by native and denaturing top-down mass spectrometry.

Ryan N. Oates,^{1#} Linda B. Lieu,^{1#} Kristina Srzentić,² Eugene Damoc,³ Luca Fornelli^{1,4*}

¹ *Department of Chemistry and Biochemistry, University of Oklahoma, Norman, OK, USA*

² *Thermo Fisher Scientific, Reinach, Switzerland*

³ *Thermo Fisher Scientific, Bremen, Germany*

⁴ *School of Biological Sciences, University of Oklahoma, Norman, OK, USA*

these authors contributed equally

* to whom correspondence should be addressed: School of Biological Sciences, Richards Hall 411b, 730 Van Vleet oval, Norman, OK, 73109. Phone: 405-325-1483; fax: 405-325-6202; email: luca.fornelli@ou.edu

Keywords: monoclonal antibody, mAb; Orbitrap; top-down; electron transfer dissociation, ETD; ultraviolet photodissociation, UVPD; native mass spectrometry; higher-energy collisional dissociation, HCD; EThcD.

Running title: native versus denaturing antibody MS analysis

ABSTRACT

Established in recent years as an important approach to unraveling the heterogeneity of intact monoclonal antibodies, native mass spectrometry has been rarely utilized for sequencing these complex biomolecules via tandem mass spectrometry. Typically, top-down mass spectrometry has been performed starting from highly charged precursor ions obtained via electrospray ionization under denaturing conditions (i.e., in the presence of organic solvents and acidic pH). Here we systematically benchmark four distinct ion dissociation methods – namely higher-energy collisional dissociation, electron transfer dissociation, electron transfer dissociation/higher-energy collisional dissociation, and 213 nm ultraviolet photodissociation – in their capability to characterize a therapeutic monoclonal antibody, trastuzumab, starting from denatured and native-like precursor ions. Interestingly, native top-down mass spectrometry results in higher sequence coverage than the experiments carried out under denaturing conditions, with the exception of ultraviolet photodissociation. Globally, electron transfer dissociation followed by collision-based activation of product ions generates the largest number of backbone cleavages in disulfide protected regions, including the complementarity determining regions, regardless of electrospray ionization conditions. Overall, these findings suggest that native mass spectrometry can certainly be used for the gas-phase sequencing of whole monoclonal antibodies, although the dissociation of denatured precursor ions still returns a few backbone cleavages not identified in native experiments. Finally, a comparison of the fragmentation maps obtained under denaturing and

native conditions strongly points towards disulfide bonds as the primary reason behind the largely overlapping dissociation patterns.

INTRODUCTION

First introduced in 1986, therapeutic monoclonal antibodies (mAbs) have grown as a new class of biological drugs due to their high specificity and efficacy.^{1, 2} In 2022, over 115 mAbs and biosimilars have been approved by regulatory agencies, such as US Food and Drug Administration (FDA) and the European Medicine Agency (EMA), with more than 800 seeking approval.^{3, 4} These biomolecules aid in treating many diseases, including cancer,^{5, 6} autoimmune disorders,⁷ and even coronavirus infection.⁸

Mostly based on the human immunoglobulin G (IgG) scaffold, therapeutic mAbs are currently modeled after one of three different subclasses of IgGs (IgG1, IgG2, or IgG4), with IgG1 being the most common subclass used.⁹ Each mAb is a ~150 kDa biomolecule comprised of two light (Lc, ~25 kDa) and two heavy chains (Hc, ~50 kDa), held together by intra- and inter-molecular disulfide bridges,¹⁰ the arrangement of which is subclass-dependent.¹¹ Historically, two functional IgG subunits have been identified: the antigen-binding fragment (Fab) and the fragment crystallizable (Fc). The Fab is present in two identical copies (F(ab')₂) in an IgG and includes the whole Lc and the N-terminal half of the Hc. Each of these polypeptides encompasses both variable and constant regions. Among the variable regions, three short amino acid sequences, called complementarity determining regions (CDRs), are directly responsible for the recognition of a specific antigen. The Fc subunit contains the C-terminal portions

of the Hc (which is N-glycosylated) and is primarily in charge of receptor recognition.¹²

The regulatory agencies require thorough characterization of all drug products. For therapeutic IgGs, this includes the determination of the intact mass and localization of certain chemical modifications. This level of characterization faces major difficulties for mAbs due to their large size, complex structure, and the presence of post-translational modifications (PTMs), including deamidation, oxidation, and glycosylation.^{13, 14} Referred to as critical quality attributes (CQAs),¹⁵ these modifications add to the structural complexity and can impact the efficacy, stability, and immunogenicity of mAbs.^{16, 17} Due to these heterogeneities, comprehensive structural characterization, from the general amino acid sequence to evaluation of different proteoforms,¹⁸ is essential.

Mass spectrometry (MS) is an analytical technique that can be used to monitor all stages of mAb production, providing information on the primary structure, PTM localization, and higher order structures.¹⁹⁻²² While proteolysis-based approaches to the MS analysis of mAbs are typically preferred, an alternative methodology, referred to as top-down mass spectrometry (TDMS),²³ relies on limited sample handling and investigates the biomolecule in its intact form. This allows for the determination of the mAb intact mass and the simultaneous characterization of Lc and Hc – preserving the so-called chain pairing information.^{24, 25} TDMS of mAbs has historically utilized Fourier transform and time-of-flight mass analyzers^{26, 27} to detect with high resolving

power and mass-over-charge (m/z) accuracy the product ions generated by different ion activation techniques,²⁸ offering crucial proteoform-level information.

TDMS can rely on electrospray ionization performed under either denaturing (dTDMS) or near-native (nTDMS) conditions. Under dTDMS, the sample is unfolded using organic solvents and non-neutral pH conditions (typically acidic).²⁹ While dTDMS provides insight into the amino acid sequence and PTM localization, information on (biologically relevant) higher-order structures is lost.³⁰ Conversely, nTDMS is carried out using ionization solutions composed of an MS-compatible salt (usually ammonium acetate) at near neutral pH, preserving noncovalent interactions and thus higher-order structure.³¹⁻³³

Traditionally, TDMS of mAbs has been performed under denaturing ionization conditions.³⁴⁻³⁶ Over the past fifteen years, multiple ion dissociation techniques have been applied to the dTDMS of mAbs, including collision-induced dissociation (CID),³⁷ higher-energy collisional dissociation (HCD),³⁸ ultraviolet photodissociation (UVPD) with 157, 193 and 213 nm photons,³⁹ and radical-driven fragmentation techniques, namely electron capture (ECD)⁴⁰ and electron transfer dissociation (ETD)⁴¹, as well as hybrid techniques such as electron transfer dissociation/higher-energy collisional dissociation (EThcD).⁴² Given the different fragmentation mechanisms behind collision, high-energy photon, and electron-based techniques,^{37, 43, 44} a more comprehensive characterization of IgGs has been obtained by combining results derived from the use of two or more

“orthogonal” ion activation methods. When possible, UVPD-based results are coupled to those from radical-driven techniques to maximize mAb sequence coverage.^{24, 45}

Conversely, native ionization has been mostly leveraged to simplify intact mass analysis, taking advantage of the reduced charge state of mAb ions, which in turn leads to limited overlap among proteoforms (particularly, glycoforms) in the m/z space.^{46, 47} When coupled to separation techniques that do not use organic solvents, native MS has also been leveraged to distinguish mAb charge variants.⁴⁸ However, a few notable examples of the application of nTDMS to mAbs exist. The body of work by Heck and co-workers provided an overview of the fragmentation pattern of ~50 kDa Fab subunits of various types of immunoglobulins via ECD under native ionization conditions.^{49, 50} While technically produced by limited proteolysis, Fab and ~100 kDa F(ab')₂ subunits demonstrate a fragmentation behavior similar to that observed on whole mAbs due to the presence of intact disulfide bonds, as discussed by Kline *et al.*⁵¹ Zhang *et al.* reported the characterization of a native-like antigen-Fab complex using collision-, electron-, and infrared photon-based dissociation.⁵² Similarly, by using 193 nm UVPD nTDMS, Mehaffey *et al.* investigated the binding of Hemagglutinin A (HA) to a specific intact mAb. While the focus of this study was the mapping of the epitopes of HA, the authors reported a notable 45% and 37% sequence coverage for the antibody Lc and Hc, respectively.⁵³ Recently, ECD has been used to perform nTDMS on a ~600 kDa pentameric IgM antibody,⁵⁴ and on an intact IgG1. The latter study by Loo and co-workers likely represents the most

comprehensive attempt to the gas-phase sequencing of a mAb ionized under native-like conditions to date, where canonical termini-containing product ions have been assigned along with internal fragments.⁵⁵

Despite the promising results obtained in the gas-phase sequencing of mAbs via nTDMS, a systematic comparison of the fragmentation results from multiple ion activation techniques on the same mAb ionized under denaturing and native conditions has yet to be accomplished. Herein, we discuss the results of the analysis of a therapeutic mAb, trastuzumab, carried out under denaturing and native conditions on a tribrid Orbitrap instrument with extended m/z range (Orbitrap Eclipse).⁵⁶ We benchmark the performance of multiple ion activations – namely HCD, ETD, EThcD and 213 nm UVPD – in dTDMS and nTDMS experiments, with specific focus on the cleavage of backbone bonds within cysteine residues involved in intra-molecular disulfide bridges.⁵⁷ These regions, which include CDRs 1 and 2, are of key importance in antibody characterization.⁵⁸ Our results demonstrate that, contrary to common beliefs, nTDMS can even outperform dTDMS, likely due to reduced spectral congestion that facilitates product ion assignment.

EXPERIMENTAL SECTION

Sample preparation – Trastuzumab (commercially sold as Herceptin; Genentech, South San Francisco, CA) was desalted in two consecutive steps using micro Bio-Spin 6 columns (Bio-Rad, Hercules, CA). The sample was buffer exchanged to a final concentration of ~5 μ M. For dTDMS, the spray solution consisted of 49.9%/49.9%/0.2% water, acetonitrile and formic acid (v/v/v); samples for nTDMS were electrosprayed in a 50 mM solution of ammonium acetate, with pH adjusted to ~7.4.

Orbitrap mass spectrometry – All MS measurements were performed on an Orbitrap Eclipse tribrid mass spectrometer (Thermo Scientific, San Jose, CA) equipped with HMRn option to allow ion detection up to m/z 8000. Samples were ionized via direct infusion using coated borosilicate emitters fitted onto a Nanospray Flex ionization source (Thermo Scientific). Spray voltage was set to 1700-2100 V. Ion desolvation was facilitated by setting the heated inlet capillary temperature at 350 °C, while declustering and adduct removal was obtained via in-source CID (set to 50-100 V). Measurements were carried out in “standard” pressure mode for both dTDMS and nTDMS. Broadband MS spectra (MS^1) were collected at resolving power (RP) of 15,000 or 30,000 (at m/z 200). Tandem MS spectra (MS^2) were collected at 240,000 RP (at m/z 200) over an m/z 300-8000 window. For MS^2 experiments, a single charge state was isolated in the linear ion trap (LTQ), with isolation centered at m/z 3026 for dTDMS (corresponding to the 49+ charge state; isolation width: 60 m/z units) and at m/z 5490 for nTDMS

(27+ charge state; isolation width: 100 m/z units). 10 time-domain transients (i.e., “microscans”) were averaged per mass spectrum, and data collection was carried out in “full profile” mode (i.e., without noise thresholding). ETD and 213 nm UVPD durations and HCD normalized collision energies (NCE) were varied during acquisition, and these parameters were differentiated for dTDMS and nTDMS (specific values are indicated in **Table S1**).

Data analysis – MS² spectra utilized for analysis were obtained by averaging 25 individual spectra (corresponding to 250 transients) in QualBrowser (Thermo Scientific). Product ion matching and manual validation was performed using TDValidator (Proteinaceous, Inc, Evanston, IL),⁴⁵ which uses an isotope fitting algorithm to match experimental ion isotopic clusters against *in silico* generated ion isotopic clusters based on the molecular formulae of theoretical fragment ions. The following settings were used: peak picking signal-to-noise ratio (S/N) threshold of 10; fragment ion tolerance, 10 ppm; inter-isotopic tolerance, 3 ppm; product ion maximum charge state, +25; minimum similarity score, 0.5. During manual validation, a minimum of 4 isotopologues of large ion clusters (i.e., corresponding to fragments >5 kDa) had to be matched for the product ion to be included in the validated list. The following ion types were searched for these ion activation methods: HCD, b^- and y^- -ions; ETD, c^- and z^- -ions; EThcD, b^- , c^- , y^- and z^- -ions; UVPD, 9 ions types (namely a^- , a^{+-} , b^- , c^- , x^- , x^{+-} , y^- , y^{--} , and z^- ions) as previously described.⁵⁹ Product ion abundance (PIA) analysis comprised only validated fragments and was performed as previously described.³⁵ Briefly, all fragment ions referring to the same

backbone cleavage were grouped, and intensities (obtained from the TDValidator report) were divided over the related product ion's charge state. Then, charge-normalized intensities of each group were summed. Finally, backbone cleavage intensities were expressed as relative percentages of the backbone cleavage with the highest intensity. PIA analysis was performed in Excel (Microsoft, Redmond, WA) and histograms were generated using GraphPad Prism 9 (GraphPad Software, San Diego, CA).

RESULTS AND DISCUSSION

Features of different ion dissociation techniques in dTDMS versus nTDMS experiments – The selection of precursor ions in this comparative analysis reflected the differences in the charge state envelopes obtained for trastuzumab under denaturing and native electrospray ionization (**Figure S1**). For dTDMS, the 49+ charge state (m/z 3026) was selected being the most intense charge state within the broad charge state distribution (spanning from 26+ to 62+). In the case of nTDMS, the 27+ charge state (m/z 5490) was isolated using a 100 m/z -wide isolation window. We opted for the use of broad isolation windows to maintain good ion isolation efficiency in the LTQ in the high m/z range.

Figure 1 shows a selection of the analyzed MS² spectra acquired under denaturing (left column) and native (right column) conditions. As reported in **Table S1**, for both dTDMS and nTDMS experiments, ETD and UVPD data were collected using three different durations. Represented in **Figure 1** is a single duration (details in the figure caption).

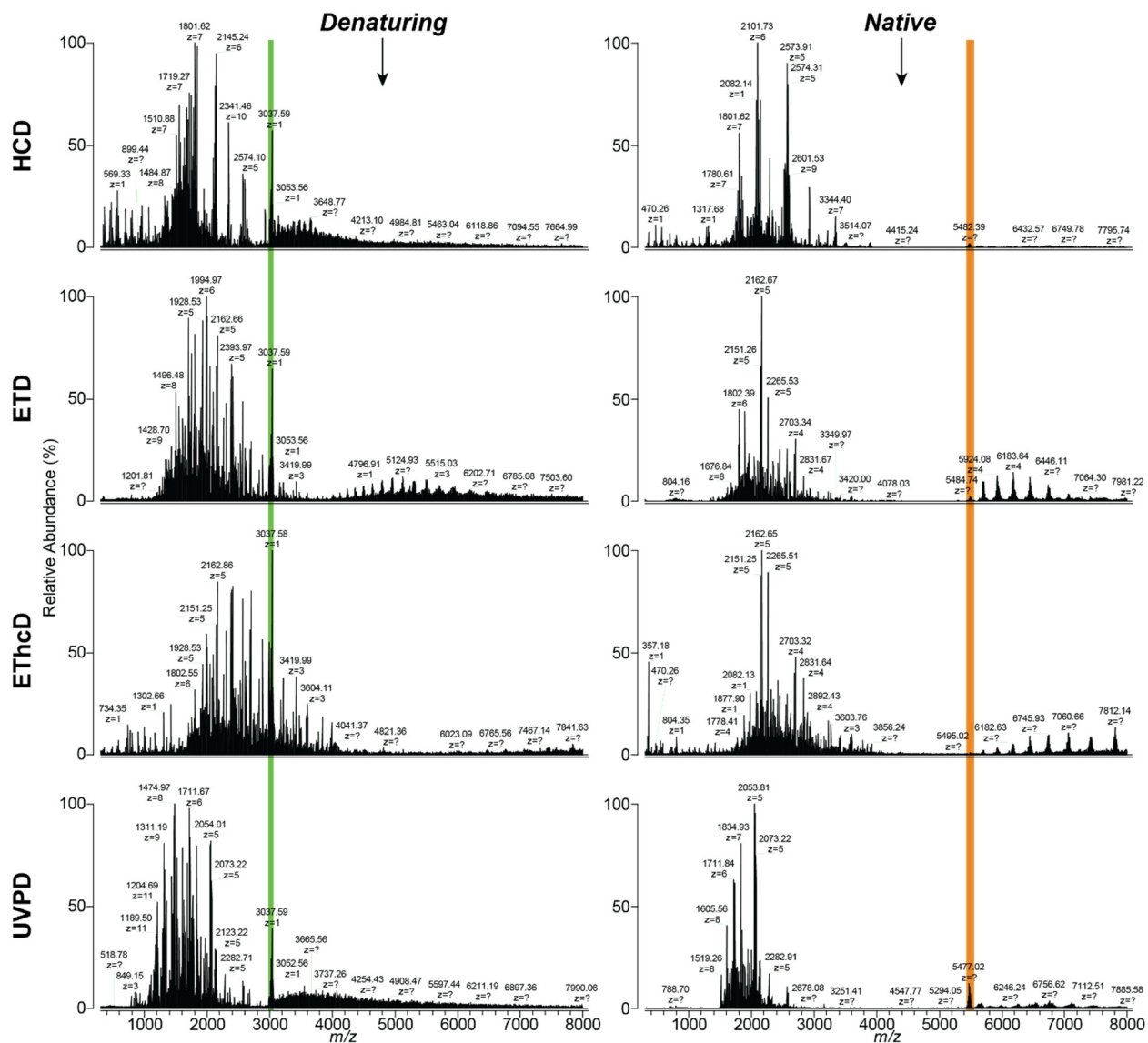


Figure 1. MS² spectra of trastuzumab recorded from precursors obtained under denaturing (left column) and native (right column) electrospray ionization conditions. The original precursor *m/z* position is indicated by colored bars. ETD spectra were acquired at duration of 5 ms (dTDMS) and 30 ms (nTDMS). UVPD spectra show the result of a 30 ms irradiation period for both dTDMS and nTDMS.

The most striking observation is the overall similarity of the spectra produced by a given fragmentation method under denaturing and native conditions. In other words, once fragmentation parameters were adjusted to account for the different charge state of the precursor, each ion dissociation led to MS² spectra that share several key features in dTDMS and nTDMS. In the case of HCD, NCE had to be substantially increased passing from denaturing to native conditions (for the reported spectra, the value was increased from 60% to 150%). Still, both the dTDMS and nTDMS spectra show the presence of lowly charged, low m/z species (largely absent or of substantially lower intensity in the MS² spectra generated by the other tested ion fragmentation methods, with the exception of EThcD), followed by another sub-population of highly charged product ions that is distinctly positioned in the m/z space (centered around m/z 1500 for dTDMS and m/z 2000 for nTDMS). The presence of two distinct ion populations is reflected in the violin plots describing the distribution of charge states of identified fragments (**Figure S2**). ETD shows a single population of sequence informative product ions (i.e., not including charge reduced species), centered around m/z values that increase with the applied ion-ion duration. As expected, EThcD spectra combine features from both ETD and HCD, and they generally include highly charged product ions (spread across a broader range than in ETD spectra) together with a sub-population of low m/z fragments (similarly to HCD spectra). Finally, UVPD generates a narrow m/z distribution of product ions, regardless of the duration of photon irradiation. Notably, optimal results for both dTDMS and nTDMS were obtained using the same three UVPD

duration times (namely 20, 30 and 40 ms). This leads us to hypothesize that the gas-phase cross-section of a highly charged, “denatured” IgG1 and of its “native-like” counterpart are not dramatically different. Reports from ion mobility mass spectrometry analysis of whole IgGs seem to support this hypothesis. A study by Campuzano *et al.* on the NIST standard mAb ionized under native conditions demonstrated that collisional cross-section values of various charge states within the same charge state envelope differ in a measurable fashion, but such differences are <5% (e.g., the Ω_{N_2} was calculated as 7223 Å² for the 21+ charge state of the NIST mAb, and as 7275 Å² for the 22+, a relative difference of 0.7%).⁶⁰ Additionally, a recent study by Gozzo *et al.* showed that differences in collisional cross-section between immunoglobulins of different classes (i.e., IgG1 versus IgG4) increase as the charge state of the ions is reduced via cation-to-anion proton-transfer reactions. However, the same study also documented that other intact proteins, such as bovine serum albumin, suffer larger changes in collisional cross-section compared to both IgG1 and IgG4 as their charge state is reduced via deprotonation.⁶¹ Taken together, these data suggest that mAb denaturation likely occurs when, by using organic solvents and low pH, the degree of protonation increases, but the variation in cross-section among charge states is likely limited by the network of intra- and inter-molecular disulfide bonds.

Table 1 summarizes the sequencing results of dTDMS and nTDMS experiments. Surprisingly, fragmentation performed under native-like conditions outperformed the corresponding dTDMS experiments for HCD and ETD, while

ETHcD returns essentially identical numbers. UVPD, on the other hand, benefitted from the isolation of a highly charged precursor. However, the effect is noticeable only on the Hc, where UVPD returns 6% higher sequence coverage in dTMDS than in nTDMS, reaching 25% (the highest value of any ion dissociation method for the Hc) thanks to a series of large product ions derived from the rupture of backbone cleavages in the center of the polypeptide chain. Conversely, the Lc sequence coverage was higher in nTDMS.

Table 1. Sequence coverage obtained after manual validation of dTDMS and nTDMS tandem mass spectra. Values are reported for the Lc, the Hc, and the antibody as a whole.

Ion Activation Technique	Light Chain		Heavy Chain		Whole IgG	
	Sequence Coverage					
	Denatured	Native	Denatured	Native	Denatured	Native
HCD	17.4	32.9	14.5	20.5	15.48	24.58
ETD ^a	19	26	17	19	17.70	21.32
ETHcD	29.1	34.7	19.9	16.4	22.94	22.37
UVPD ^b	31	32	25	19	27.02	23.27
Total Coverage	60		44		49.31	

This finding is mirrored by the number of unique matched product ions, which are often higher in nTDMS experiments (**Table S1**). The only exception to this trend is again UVPD. As mentioned, UVPD led to the formation of sequence informative product ions with the highest average mass of any tested ion dissociation technique in dTDMS (**Table S2**), and the average mass of UVPD fragments for Lc and Hc remains essentially unchanged in nTDMS experiments (where ETD produced the largest fragments). The relative frequency of the 9

product ion types generated by UVPD is also essentially identical in dTDMS and nTDMS (**Figure S3**). This, together with the fact that increased irradiation times in nTDMS experiments resulted only minor differences in sequence coverage, likely indicates that the observed differences in sequence coverage between denaturing and native UVPD experiments are to be ascribed at least in part to the charge state of the precursor: additional fragmentation channels may be available in the case of precursors with higher charge density, particularly for the Hc. This hypothesis is supported by the analysis of matched product ions by irradiation time (**Figure S4**). UVPD nTDMS experiments produce largely the same product ions regardless of irradiation time, especially in the case of the Lc. Conversely, significant changes are induced by the variation of ultraviolet photon irradiation time in the case of dTDMS, for both the light and the heavy chain. When considering the overall sequence coverage for the whole IgG, UVPD provided by far the highest sequence coverage of any ion fragmentation method in dTDMS experiments (27%), but just in line with the other methods in nTDMS (23.3%), where EThcD outperformed it (24.6%).

Comparatively, in ETD the variation of ion-ion reaction times (3, 5 and 10 ms for dTDMS; 10, 20 and 30 ms for nTDMS) led to modest differences in the assigned product ions (**Figure S5**). The increase in sequence coverage achieved by moving from ETD dTDMS to ETD nTDMS was notable: the light chain sequence coverage went from 19% to 26%, and from 17% to 19% in the case of the heavy chain.

HCD results largely mimic those of ETD. The increase in sequence coverage was significant moving from denaturing to native conditions (light chain sequence coverage: from 17.4% to 32.9%; heavy chain: from 14.5% to 20.5%). Surprisingly, HCD outperformed ETD in overall sequence coverage under native-like conditions (24.6% and 21.3% for HCD and ETD, respectively), but produced the lowest coverage of any fragmentation method in dTDMS (15.5%). This seemingly confirms previous reports demonstrating an inverse correlation between sequence coverage produced via HCD and charge density of the intact protein precursor ion.^{59, 62} Notably, the optimal HCD NCE for trastuzumab in both dTDMS and nTDMS was higher than for a typical intact protein, at 60% and 150%, respectively. This presumably reflects the relatively compact conformation that IgG ions maintain in the gas-phase due to the presence of disulfide bridges.

ETHcD has been proven previously to produce sequencing results similar to ETD for intact mAbs, but also to produce additional fragment ions compared to ETD.³⁵ In this test, ETHcD carried out with a single set of parameters (i.e., one ETD duration and one HCD voltage for supplemental activation of ETD products) returned high sequence coverage and was outperformed only by the combination of three UVPD experiments with varying durations in dTDMS (total sequence coverage of 22.9% for ETHcD, versus 27% for UVPD). In nTDMS, mAb sequencing results were closer among three of the four fragmentation methods, with ETHcD, UVPD and HCD resulting in 22.3%, 23.2%, and 24.6% global sequence coverage, respectively. Curiously, the collisional re-activation of product ions generated by

ETD is reflected in the relatively low averaged mass of matched product ions (the lowest of any considered ion activation, as detailed in **Table S2** and displayed in **Figure S2**), which is likely not explained solely by the relatively long ETD duration applied (i.e., 10 ms for dTDMS, the highest duration used in regular ETD experiments; 30 ms for nTDMS, the middle value of the three used for regular ETD). Arguably, product ions with reduced mass and low charge state are less prone to overlap in the m/z space, facilitating their assignment.

Overall, the sequence coverage obtained by a given ion dissociation method did not change dramatically between dTDMS and nTDMS, with perhaps the only exception of HCD. However, this observation does not fully recapitulate possible differences in the actual fragmentation patterns. In **Figure 2**, Venn diagrams compare unique product ions (as neutral masses) assigned under denaturing and native-like experimental conditions, demonstrating that, in general, a large fraction of assigned fragments are unique for either dTDMS or nTDMS. However, differences exist among ion dissociation methods. Specifically, ETD led to similar fragmentation between the two tested conditions, but mainly because the population of product ions matched in nTDMS is substantially larger than the dTDMS counterpart and includes most of the fragments identified in dTDMS experiments. The only cases when half or more of the total number of identified fragments was shared between dTDMS and nTDMS experimental sets were for ETD (Lc: 52.7%; Hc: 58.8%) and for the Lc analyzed via UVPD (50%). While the fact that ETD (as well as HCD) produces mainly just two ion types (i.e., c - and z -ions) may favor a higher degree of similarity between the fragmentation patterns

observed in dTDMS and nTDMS, the homogeneity of ETD fragmentation regardless of precursor ion characteristics is still remarkable when considering that a total of six different ion-ion reaction durations were employed in ETD experiments.

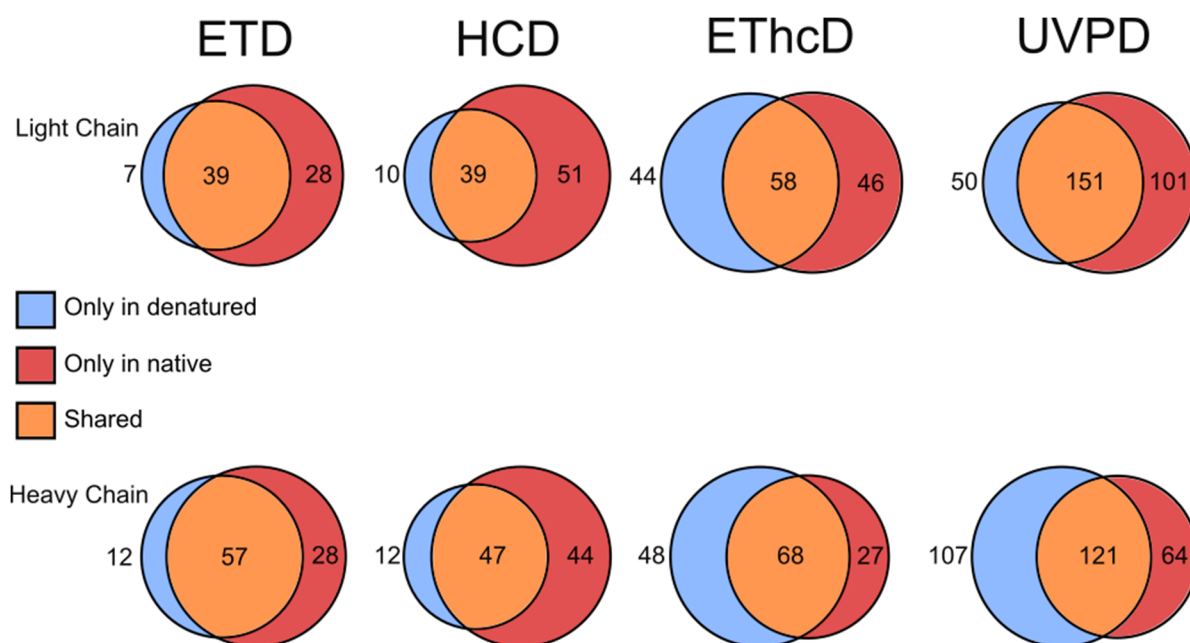


Figure 2. Venn Diagram of unique product ions of each ion activation method. Red shows native-only product ions, blue shows denatured-only product ions, and orange shows shared product ions. Product ions were considered as neutral masses; hence, differences in charge states of assigned fragments are not accounted for in the Venn diagrams.

In general, at least 39% of matched fragments are shared between dTDMS and nTDMS. Such results support the notion that fragmentation in intact antibodies is primarily driven by the position of disulfide bonds, as previously reported.^{35, 45} In the case of EThcD, fragments uniquely identified in one of the

experimental sets are evenly distributed between dTDMS and nTDMS. A simple visual comparison of the EThcD dTDMS and nTDMS spectra shows that many of the most abundant product ions are identical (i.e., not only derived from the same backbone position, but also having the same charge state), while the differences primarily involve low abundant fragments (**Figure S6**).

Global antibody sequencing results – The slightly reduced product ion signal overlap may explain also the overall higher sequence coverage obtained by the nTDMS experiments. By combining the assigned backbone cleavages from all individual experiments, the sequence coverage for the whole antibody reaches 37.7% and 43.6% for dTDMS and nTDMS, respectively (**Table S1**). The total sequence coverage obtained by merging dTDMS and nTDMS data is 49.3% (**Tables 1** and **S1**). As shown in the combined fragmentation map in **Figure 3**, the overall sequence coverage for the light chain is 60%, with particularly high coverage of the region preceding the third Cys residue (Cys₁₃₄).

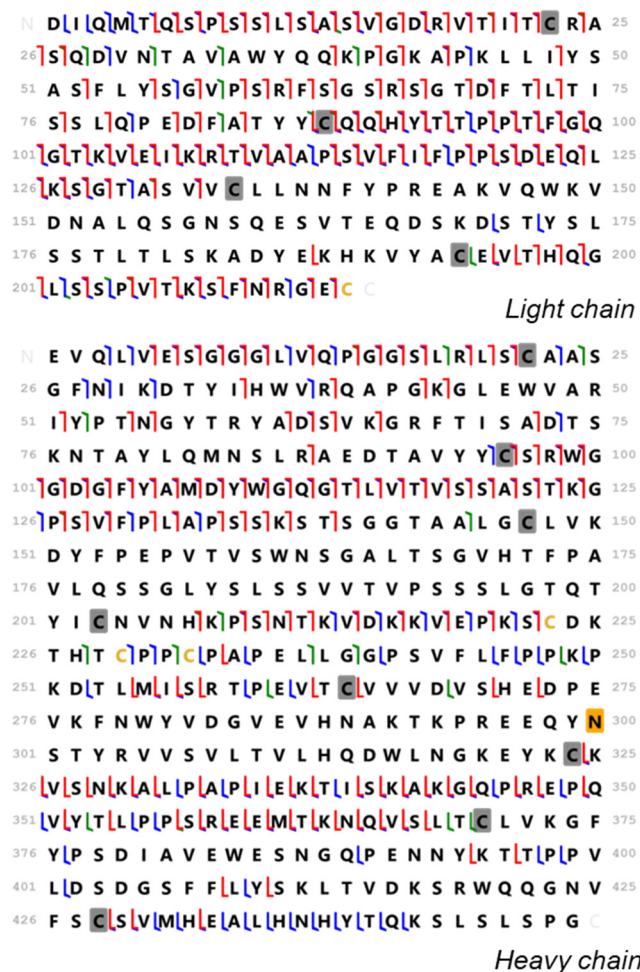


Figure 3. Combined fragmentation maps of the light and heavy chain of trastuzumab including all matched product ions from dTDMS and nTDMS experiments. Color scheme: green, *a*/*x*-ions; blue, *b*/*y*-ions; red, *c*/*z*-ions.

The relatively high sequence coverage obtained for the heavy chain can be attributed mostly to the experiments performed under native-like conditions, which allow for the assignment of backbone cleavages positioned within two portions of the Hc not well characterized by dTDMS. The first of these regions is the central portion of the Hc, between residues Cys₂₀₃ and Cys₂₆₄. **Figure S7**, which compares the global fragmentation results for dTDMS versus nTDMS

experiments, shows 26 matched backbone cleavages from dTDMS versus 30 from nTDMS within that region. The second region will be discussed below.

Characterization of CDRs and disulfide protected regions – CDRs are part of the variable domains of both Lc and Hc. Both denaturing and native-like top-down MS experiments led to extensive sequencing of CDR3,^{24, 45, 49} which is part of the loop positioned between the first and second disulfide-protected regions of either mAb chain. On the contrary, being protected by a disulfide bond, CDRs 1 and 2 are usually harder to characterize. The present study confirms this trend, with the only fully sequenced CDR of trastuzumab being CDR3 (**Table 2**). ETD, EThcD, and UVPD were equally capable of returning 100% sequence coverage of the CDR3 in the Hc (amino acid residues 100-110), while electron-based fragmentation methods reached only 75% coverage of CDR3 in the Lc (amino acid residues 89-97) due to the presence of two consecutive Pro residues. Unfortunately, HCD was incapable of producing good sequencing of any CDR of either chain of trastuzumab.

Table 2. Sequence coverage of CDR regions per fragmentation method under denaturing and native conditions.

Ion Activation Technique	Denatured						Native					
	Light Chain			Heavy Chain			Light Chain			Heavy Chain		
	Sequence Coverage (%)											
	CDR1	CDR2	CDR3	CDR1	CDR2	CDR3	CDR1	CDR2	CDR3	CDR1	CDR2	CDR3
HCD	0	0	25	0	0	50	10	0	62.5	11.1	6.3	40
ETD	0	0	75	0	0	100	10	0	75	0	25	100
EThcD	10	16.7	50	11.1	6.3	100	10	16.7	75	11.1	31.3	100
UVPD	20	0	100	0	6.3	100	40	0	100	11.1	0	100
Combined	30	16.7	100	11.1	12.5	100	60	16.7	100	33.3	43.8	100

CDRs 1 and 2 are not only located within a disulfide bond, but CDR2 of the Hc is also particularly long (residues 50-66). In dTDMS, the only ion activation technique that led to acceptable characterization of these regions was EThcD, which struggled only with the above mentioned CDR2 of the Hc (6.3% coverage, equivalent to only 1 assigned backbone cleavage out of 16). UVPD produced results only for CDR1 of the Lc and CDR2 of the Hc. Overall, the regions corresponding to CDRs 1 and 2 of the Hc are poorly sequenced in dTMDS. In agreement with the globally higher coverage obtained under native-like conditions, CDR characterization improved in nTDMS experiments. However, CDR sequence coverage did not increase equally for all ion dissociations. UVPD could not lead to the liberation of fragments from CDR2 even in nTDMS. The most substantial improvements were demonstrated by HCD and ETD, with the former achieving partial sequencing of all CDRs except CDR2 of the Lc. Overall, CDR2 of Lc and Hc proved the hardest to characterize even in nTDMS, with $\leq 50\%$ coverage under either ionization condition. EThcD was by far the most successful ion dissociation for sequencing CDR2 of Lc and Hc, outperforming not only ETD and UVPD in our experiments, but also improving over the results obtained via ECD in previous studies.⁴⁹ This emphasizes the relevance of supplemental activation in electron-based ion dissociation to reach deeper sequencing of disulfide-protected regions.⁶³

Despite this being a controversial topic, there is substantial evidence that vibrational energy-threshold dissociation techniques like HCD can induce the cleavage of S-S bonds. As in previous reports,^{64, 65} the present results also

demonstrate that fragment ions were produced from disulfide protected regions by collisional dissociation (i.e., HCD), both in dTDMS and nTDMS. **Figure 4** shows clear examples of such fragment ions, which unsurprisingly were produced by the rupture of backbone bonds in proximity of Pro or Asp residues.⁵⁹

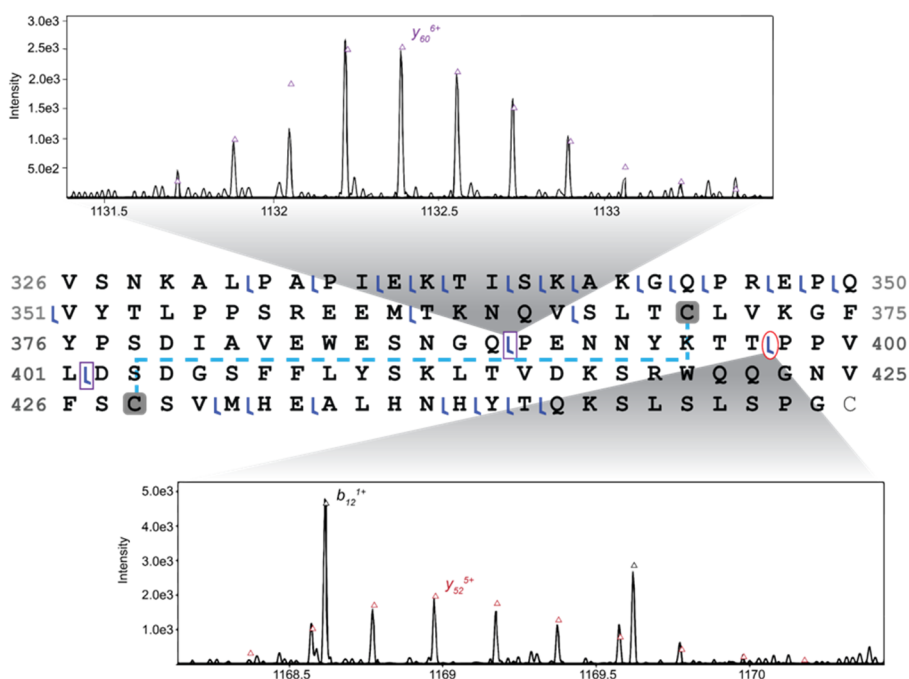


Figure 4. Selected fragment ions from the disulfide protected region within residues 370-428 of the Hc produced by HCD under denaturing conditions. Good match with theoretical isotopologues' m/z positions and relative abundances is observed.

Surprisingly, for any tested ion dissociation technique, the number (**Table S3**) and relative abundance (**Figures S8-11**) of identified fragments from disulfide protected regions are always higher in native-like experiments compared to dTMDS. The only partial exception is UVPD, for which the total number of matched fragments increases moving from dTMDS to nTDMS, but not

for both antibody chains (nTDMS returns +4 fragments from the Lc and -2 from the Hc compared to dTMDS). Following the same trend discussed with regard to the sequencing of CDRs, EThcD is the dissociation method that in general produced the highest number of fragment identifications from disulfide protected regions, including 23 just from the Lc in nTDMS experiments. **Figure 5** exemplifies the capability of EThcD of inducing the formation of both *b/y*- and *c/z*-type product ions from S-S protected regions.

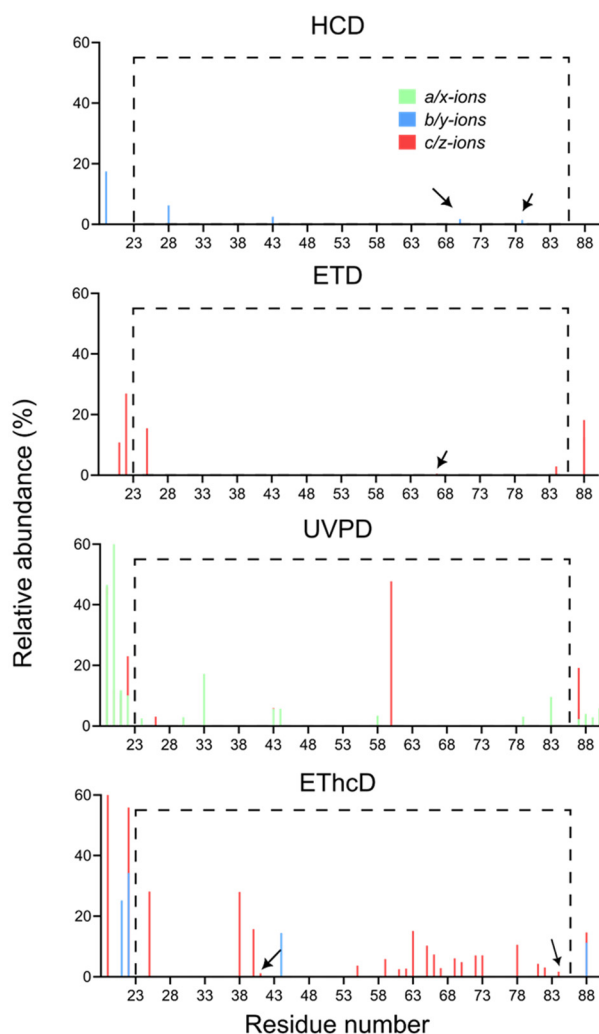


Figure 5. Product ion abundance analysis highlighting fragment ions generated by nTDMS located within the disulfide bond between residues 23-86 of the Lc. Green lines represent *a/x*-type ions, blue *b/y*-type ions, and red *c/z*-type ions. Black dashed lines represent disulfide bonded residues. Low abundant ions are indicated by the presence of arrows.

Product ion abundance analysis (PIA) demonstrates that, on average, the relative intensity of product ions from these regions remains low regardless of the ion activation method. However, UVPD and EThcD resulted in backbone cleavages that, for a few amino acid pairs, reached a total fragment intensity $\geq 20\%$ relative to the cleavage sites with the most abundant product ions of the respective experiments.

CONCLUSIONS

Although often considered as not optimal for polypeptide sequencing, nTDMS was proven here to be globally superior to dTDMS for the characterization of intact mAbs. This is likely due to two intertwined factors: the first is that the fragmentation of whole antibodies is drastically limited by the presence of disulfide bonds, which prevent complete unfolding of precursor ions even when denaturing conditions are applied. Second, in dTDMS the higher protonation of precursor ions results primarily in a broader distribution of charge states of the same abundant fragments derived from the cleavage of disulfide-free regions compared to nTDMS. Conversely, nTDMS spectra suffer less from ion signal overlap and allow for the identification of lowly abundant

product ions. This is demonstrated by the percentage of unique product ion masses over the total number of identified product ions. It is apparent that in nTDMS fewer charge states of the same fragment are generated (**Table S4**). This holds true for every scenario except in the case of the Hc sequenced via UVPD and ETD, where dTDMS produced a higher percentage of unique fragments.

In summary, monoclonal antibodies represent a structurally peculiar class of proteins for which native MS could and possibly should be used not only for intact mass determination, but also for gas-phase sequencing. This does not mean that dTDMS necessarily generates fewer fragment ions than nTDMS, but most likely the former would benefit from spectral simplification (for instance, obtained via the application of proton transfer reactions combined with ion parking)⁶⁶ in order to show its full potential.

SUPPORTING INFORMATION

Sequence coverage and unique ion count of trastuzumab for each fragmentation experiment; summary of unique product ion count and average mass (Da) per fragmentation technique; average mass and count of unique product ions per fragmentation technique located within disulfide-protected regions; fraction of unique product ions per fragmentation method; MS¹ spectra of trastuzumab ionized under denaturing and native conditions; mass distribution of matched product ions; fragment ion count from UVPD MS2 experiments under denaturing and native ionization conditions; Venn diagrams comparing unique ion counts of individual UVPD experiments with different durations; Venn diagrams

comparing unique ion counts of individual ETD experiments with different durations; comparison of EThcD MS² spectra obtained under denaturing and native conditions; global fragmentation maps obtained from dTDMS and nTDMS; product ion abundance histograms of HCD-produced product ions of each mAb chain; product ion abundance histograms of ETD-produced product ions of each mAb chain; product ion abundance histograms of EThcD-produced product ions of each mAb chain; product ion abundance histograms of UVPD-produced product ions of each mAb chain.

AUTHOR INFORMATION

Corresponding Author

*Luca Fornelli: School of Biological Sciences, University of Oklahoma, 730 Van Vleet oval, Richards Hall 411b, Norman, Oklahoma 73019; e-mail: luca.fornelli@ou.edu; phone: 405-325-1483; fax: 405-325-6202.

ORCID

Kristina Srzentić: 0000-0002-7098-1460

Luca Fornelli: 0000-0001-6334-1046

NOTES

The authors declare the following competing financial interest: K.S. and E.D. are employees of Thermo Fisher Scientific, which commercializes the instrument used in this study.

ACKNOWLEDGEMENTS

This work has been supported by the National Institute of General Medical Sciences of the National Institutes of Health under Award Number R35GM147397 to L.F. The content is solely the responsibility of the authors and does not necessarily represent the official views of the National Institutes of Health.

REFERENCES

1. Yamada, T. Therapeutic monoclonal antibodies. *Keio J Med* **2011**, *60* (2), 37-46.
2. Castelli, M. S.; McGonigle, P.; Hornby, P. J. The pharmacology and therapeutic applications of monoclonal antibodies. *Pharmacol Res Perspect* **2019**, *7* (6), e00535.
3. Kaplon, H.; Chenoweth, A.; Crescioli, S.; Reichert, J. M. Antibodies to watch in 2022. *MAbs* **2022**, *14* (1), 2014296.
4. Mullard, A. FDA approves 100th monoclonal antibody product. *Nat Rev Drug Discov* **2021**, *20* (7), 491-495.
5. Adams, G. P.; Weiner, L. M. Monoclonal antibody therapy of cancer. *Nat Biotechnol* **2005**, *23* (9), 1147-57.
6. Hafeez, U.; Gan, H. K.; Scott, A. M. Monoclonal antibodies as immunomodulatory therapy against cancer and autoimmune diseases. *Curr Opin Pharmacol* **2018**, *41*, 114-121.
7. Lu, R. M.; Hwang, Y. C.; Liu, I. J.; Lee, C. C.; Tsai, H. Z.; Li, H. J.; Wu, H. C. Development of therapeutic antibodies for the treatment of diseases. *J Biomed Sci* **2020**, *27* (1), 1.
8. Shanmugaraj, B.; Siri wattananon, K.; Wangkanont, K.; Phoolcharoen, W. Perspectives on monoclonal antibody therapy as potential therapeutic intervention for Coronavirus disease-19 (COVID-19). *Asian Pac J Allergy Immunol* **2020**, *38* (1), 10-18.
9. Beck, A.; Liu, H. Macro- and Micro-Heterogeneity of Natural and Recombinant IgG Antibodies. *Antibodies (Basel)* **2019**, *8* (1).
10. Liu, H.; Chumsae, C.; Gaza-Bulseco, G.; Hurkmans, K.; Radziejewski, C. H. Ranking the susceptibility of disulfide bonds in human IgG1 antibodies by reduction, differential alkylation, and LC-MS analysis. *Anal Chem* **2010**, *82* (12), 5219-26.
11. Liu, H.; May, K. Disulfide bond structures of IgG molecules: structural variations, chemical modifications and possible impacts to stability and biological function. *MAbs* **2012**, *4* (1), 17-23.
12. Delidakis, G.; Kim, J. E.; George, K.; Georgiou, G. Improving Antibody Therapeutics by Manipulating the Fc Domain: Immunological and Structural Considerations. *Annu Rev Biomed Eng* **2022**, *24*, 249-274.
13. Xu, Y.; Wang, D.; Mason, B.; Rossomando, T.; Li, N.; Liu, D.; Cheung, J. K.; Xu, W.; Raghava, S.; Katiyar, A.; Nowak, C.; Xiang, T.; Dong, D. D.; Sun, J.; Beck,

- A.; Liu, H. Structure, heterogeneity and developability assessment of therapeutic antibodies. *MAbs* **2019**, *11* (2), 239-264.
14. Higel, F.; Seidl, A.; Sorgel, F.; Friess, W. N-glycosylation heterogeneity and the influence on structure, function and pharmacokinetics of monoclonal antibodies and Fc fusion proteins. *Eur J Pharm Biopharm* **2016**, *100*, 94-100.
 15. Alt, N.; Zhang, T. Y.; Motchnik, P.; Taticek, R.; Quarmby, V.; Schlothauer, T.; Beck, H.; Emrich, T.; Harris, R. J. Determination of critical quality attributes for monoclonal antibodies using quality by design principles. *Biologicals* **2016**, *44* (5), 291-305.
 16. Wang, W.; Singh, S.; Zeng, D. L.; King, K.; Nema, S. Antibody structure, instability, and formulation. *J Pharm Sci* **2007**, *96* (1), 1-26.
 17. Jefferis, R. Posttranslational Modifications and the Immunogenicity of Biotherapeutics. *J Immunol Res* **2016**, *2016*, 5358272.
 18. Smith, L. M.; Kelleher, N. L.; Consortium for Top Down, P. Proteoform: a single term describing protein complexity. *Nat Methods* **2013**, *10* (3), 186-7.
 19. Rosati, S.; Thompson, N. J.; Heck, A. J. R. Tackling the increasing complexity of therapeutic monoclonal antibodies with mass spectrometry. *Trac-Trend Anal Chem* **2013**, *48*, 72-80.
 20. Zhang, H.; Cui, W.; Gross, M. L. Mass spectrometry for the biophysical characterization of therapeutic monoclonal antibodies. *FEBS Lett* **2014**, *588* (2), 308-17.
 21. Beck, A.; Sanglier-Cianferani, S.; Van Dorsselaer, A. Biosimilar, biobetter, and next generation antibody characterization by mass spectrometry. *Anal Chem* **2012**, *84* (11), 4637-46.
 22. Ladwig, P. M.; Barnidge, D. R.; Willrich, M. A. V. Mass Spectrometry Approaches for Identification and Quantitation of Therapeutic Monoclonal Antibodies in the Clinical Laboratory. *Clin Vaccine Immunol* **2017**, *24* (5).
 23. Toby, T. K.; Fornelli, L.; Kelleher, N. L. Progress in Top-Down Proteomics and the Analysis of Proteoforms. *Annu Rev Anal Chem (Palo Alto Calif)* **2016**, *9* (1), 499-519.
 24. Shaw, J. B.; Liu, W.; Vasil Ev, Y. V.; Bracken, C. C.; Malhan, N.; Guthals, A.; Beckman, J. S.; Voinov, V. G. Direct Determination of Antibody Chain Pairing by Top-down and Middle-down Mass Spectrometry Using Electron Capture Dissociation and Ultraviolet Photodissociation. *Anal Chem* **2020**, *92* (1), 766-773.
 25. Srzentic, K.; Nagornov, K. O.; Fornelli, L.; Lobas, A. A.; Ayoub, D.; Kozhinov, A. N.; Gasilova, N.; Menin, L.; Beck, A.; Gorshkov, M. V.; Aizikov, K.; Tsybin, Y. O. Multiplexed Middle-Down Mass Spectrometry as a Method for Revealing Light and Heavy Chain Connectivity in a Monoclonal Antibody. *Anal Chem* **2018**, *90* (21), 12527-12535.
 26. Bondarenko, P. V.; Second, T. P.; Zabrouskov, V.; Makarov, A. A.; Zhang, Z. Mass measurement and top-down HPLC/MS analysis of intact monoclonal antibodies on a hybrid linear quadrupole ion trap-Orbitrap mass spectrometer. *J Am Soc Mass Spectrom* **2009**, *20* (8), 1415-24.
 27. Tsybin, Y. O.; Fornelli, L.; Stoermer, C.; Luebeck, M.; Parra, J.; Nallet, S.; Wurm, F. M.; Hartmer, R. Structural analysis of intact monoclonal antibodies by electron transfer dissociation mass spectrometry. *Anal Chem* **2011**, *83* (23), 8919-27.
 28. Macias, L. A.; Santos, I. C.; Brodbelt, J. S. Ion Activation Methods for Peptides and Proteins. *Anal Chem* **2020**, *92* (1), 227-251.
 29. Donnelly, D. P.; Rawlins, C. M.; DeHart, C. J.; Fornelli, L.; Schachner, L. F.; Lin, Z.; Lippens, J. L.; Aluri, K. C.; Sarin, R.; Chen, B.; Lantz, C.; Jung, W.; Johnson, K. R.; Koller, A.; Wolff, J. J.; Campuzano, I. D. G.; Auclair, J. R.; Ivanov, A. R.; Whitelegge, J. P.; Pasa-Tolic, L.; Chamot-Rooke, J.; Danis, P. O.; Smith, L. M.; Tsybin,

- Y. O.; Loo, J. A.; Ge, Y.; Kelleher, N. L.; Agar, J. N. Best practices and benchmarks for intact protein analysis for top-down mass spectrometry. *Nat Methods* **2019**, *16* (7), 587-594.
30. Breuker, K.; McLafferty, F. W. Stepwise evolution of protein native structure with electrospray into the gas phase, 10(-12) to 10(2) s. *Proc Natl Acad Sci U S A* **2008**, *105* (47), 18145-52.
31. Leney, A. C.; Heck, A. J. Native Mass Spectrometry: What is in the Name? *J Am Soc Mass Spectrom* **2017**, *28* (1), 5-13.
32. Konermann, L. Addressing a Common Misconception: Ammonium Acetate as Neutral pH "Buffer" for Native Electrospray Mass Spectrometry. *J Am Soc Mass Spectrom* **2017**, *28* (9), 1827-1835.
33. Konermann, L.; Liu, Z.; Haidar, Y.; Willans, M. J.; Bainbridge, N. A. On the Chemistry of Aqueous Ammonium Acetate Droplets during Native Electrospray Ionization Mass Spectrometry. *Anal Chem* **2023**, *95* (37), 13957-13966.
34. Mao, Y.; Valeja, S. G.; Rouse, J. C.; Hendrickson, C. L.; Marshall, A. G. Top-down structural analysis of an intact monoclonal antibody by electron capture dissociation-Fourier transform ion cyclotron resonance-mass spectrometry. *Anal Chem* **2013**, *85* (9), 4239-46.
35. Fornelli, L.; Ayoub, D.; Aizikov, K.; Liu, X.; Damoc, E.; Pevzner, P. A.; Makarov, A.; Beck, A.; Tsybin, Y. O. Top-down analysis of immunoglobulin G isotypes 1 and 2 with electron transfer dissociation on a high-field Orbitrap mass spectrometer. *J Proteomics* **2017**, *159*, 67-76.
36. Fornelli, L.; Damoc, E.; Thomas, P. M.; Kelleher, N. L.; Aizikov, K.; Denisov, E.; Makarov, A.; Tsybin, Y. O. Analysis of intact monoclonal antibody IgG1 by electron transfer dissociation Orbitrap FTMS. *Mol Cell Proteomics* **2012**, *11* (12), 1758-67.
37. Wells, J. M.; McLuckey, S. A. Collision-induced dissociation (CID) of peptides and proteins. *Methods Enzymol* **2005**, *402*, 148-85.
38. Olsen, J. V.; Macek, B.; Lange, O.; Makarov, A.; Horning, S.; Mann, M. Higher-energy C-trap dissociation for peptide modification analysis. *Nat Methods* **2007**, *4* (9), 709-12.
39. Brodbelt, J. S. Photodissociation mass spectrometry: new tools for characterization of biological molecules. *Chem Soc Rev* **2014**, *43* (8), 2757-83.
40. Zubarev, R. A.; Horn, D. M.; Fridriksson, E. K.; Kelleher, N. L.; Kruger, N. A.; Lewis, M. A.; Carpenter, B. K.; McLafferty, F. W. Electron capture dissociation for structural characterization of multiply charged protein cations. *Anal Chem* **2000**, *72* (3), 563-73.
41. Syka, J. E.; Coon, J. J.; Schroeder, M. J.; Shabanowitz, J.; Hunt, D. F. Peptide and protein sequence analysis by electron transfer dissociation mass spectrometry. *Proc Natl Acad Sci U S A* **2004**, *101* (26), 9528-33.
42. Brunner, A. M.; Lossel, P.; Liu, F.; Huguet, R.; Mullen, C.; Yamashita, M.; Zabrouskov, V.; Makarov, A.; Altelaar, A. F.; Heck, A. J. Benchmarking multiple fragmentation methods on an orbitrap fusion for top-down phospho-proteome characterization. *Anal Chem* **2015**, *87* (8), 4152-8.
43. Zhurov, K. O.; Fornelli, L.; Wodrich, M. D.; Laskay, U. A.; Tsybin, Y. O. Principles of electron capture and transfer dissociation mass spectrometry applied to peptide and protein structure analysis. *Chem Soc Rev* **2013**, *42* (12), 5014-30.
44. R, R. J. The Mechanism Behind Top-Down UVPD Experiments: Making Sense of Apparent Contradictions. *J Am Soc Mass Spectrom* **2017**, *28* (9), 1823-1826.
45. Fornelli, L.; Srzentic, K.; Huguet, R.; Mullen, C.; Sharma, S.; Zabrouskov, V.; Fellers, R. T.; Durbin, K. R.; Compton, P. D.; Kelleher, N. L. Accurate Sequence Analysis

of a Monoclonal Antibody by Top-Down and Middle-Down Orbitrap Mass Spectrometry Applying Multiple Ion Activation Techniques. *Anal Chem* **2018**, *90* (14), 8421-8429.

46. Rosati, S.; Yang, Y.; Barendregt, A.; Heck, A. J. Detailed mass analysis of structural heterogeneity in monoclonal antibodies using native mass spectrometry. *Nat Protoc* **2014**, *9* (4), 967-76.

47. Rosati, S.; Rose, R. J.; Thompson, N. J.; van Duijn, E.; Damoc, E.; Denisov, E.; Makarov, A.; Heck, A. J. Exploring an orbitrap analyzer for the characterization of intact antibodies by native mass spectrometry. *Angew Chem Int Ed Engl* **2012**, *51* (52), 12992-6.

48. Bailey, A. O.; Han, G.; Phung, W.; Gazis, P.; Sutton, J.; Josephs, J. L.; Sandoval, W. Charge variant native mass spectrometry benefits mass precision and dynamic range of monoclonal antibody intact mass analysis. *MABs* **2018**, *10* (8), 1214-1225.

49. den Boer, M. A.; Greisch, J. F.; Tamara, S.; Bondt, A.; Heck, A. J. R. Selectivity over coverage in de novo sequencing of IgGs. *Chem Sci* **2020**, *11* (43), 11886-11896.

50. Greisch, J. F.; den Boer, M. A.; Beurskens, F.; Schuurman, J.; Tamara, S.; Bondt, A.; Heck, A. J. R. Generating Informative Sequence Tags from Antigen-Binding Regions of Heavily Glycosylated IgA1 Antibodies by Native Top-Down Electron Capture Dissociation. *J Am Soc Mass Spectrom* **2021**, *32* (6), 1326-1335.

51. Kline, J. T.; Melani, R. D.; Fornelli, L. Mass spectrometry characterization of antibodies at the intact and subunit levels: From targeted to large-scale analysis. *Int J Mass Spectrom* **2023**, *492*.

52. Zhang, Y.; Cui, W.; Weckslers, A. T.; Zhang, H.; Molina, P.; Deperalta, G.; Gross, M. L. Native MS and ECD Characterization of a Fab-Antigen Complex May Facilitate Crystallization for X-ray Diffraction. *J Am Soc Mass Spectrom* **2016**, *27* (7), 1139-42.

53. Mehaffey, M. R.; Lee, J.; Jung, J.; Lanzillotti, M. B.; Escobar, E. E.; Morgenstern, K. R.; Georgiou, G.; Brodbelt, J. S. Mapping a Conformational Epitope of Hemagglutinin A Using Native Mass Spectrometry and Ultraviolet Photodissociation. *Anal Chem* **2020**, *92* (17), 11869-11878.

54. Greisch, J. F.; den Boer, M. A.; Lai, S. H.; Gallagher, K.; Bondt, A.; Commandeur, J.; Heck, A. J. R. Extending Native Top-Down Electron Capture Dissociation to MDa Immunoglobulin Complexes Provides Useful Sequence Tags Covering Their Critical Variable Complementarity-Determining Regions. *Anal Chem* **2021**, *93* (48), 16068-16075.

55. Wei, B.; Lantz, C.; Liu, W.; Viner, R.; Ogorzalek Loo, R. R.; Campuzano, I. D. G.; Loo, J. A. Added Value of Internal Fragments for Top-Down Mass Spectrometry of Intact Monoclonal Antibodies and Antibody-Drug Conjugates. *Anal Chem* **2023**, *95* (24), 9347-9356.

56. Yu, Q.; Paulo, J. A.; Naverrete-Perea, J.; McAlister, G. C.; Canterbury, J. D.; Bailey, D. J.; Robitaille, A. M.; Huguet, R.; Zabrouskov, V.; Gygi, S. P.; Schweppe, D. K. Benchmarking the Orbitrap Tribrid Eclipse for Next Generation Multiplexed Proteomics. *Anal Chem* **2020**, *92* (9), 6478-6485.

57. McAuley, A.; Jacob, J.; Kolvenbach, C. G.; Westland, K.; Lee, H. J.; Brych, S. R.; Rehder, D.; Kleemann, G. R.; Brems, D. N.; Matsumura, M. Contributions of a disulfide bond to the structure, stability, and dimerization of human IgG1 antibody CH3 domain. *Protein Sci* **2008**, *17* (1), 95-106.

58. Gabrielli, E.; Pericolini, E.; Cenci, E.; Ortelli, F.; Magliani, W.; Ciociola, T.; Bistoni, F.; Conti, S.; Vecchiarelli, A.; Polonelli, L. Antibody complementarity-determining regions (CDRs): a bridge between adaptive and innate immunity. *PLoS One* **2009**, *4* (12), e8187.

59. Fornelli, L.; Srzentic, K.; Toby, T. K.; Doubleday, P. F.; Huguet, R.; Mullen, C.; Melani, R. D.; Dos Santos Seckler, H.; DeHart, C. J.; Weisbrod, C. R.; Durbin, K. R.; Greer, J. B.; Early, B. P.; Fellers, R. T.; Zabrouskov, V.; Thomas, P. M.; Compton, P. D.; Kelleher, N. L. Thorough Performance Evaluation of 213 nm Ultraviolet Photodissociation for Top-down Proteomics. *Mol Cell Proteomics* **2020**, *19* (2), 405-420.
60. Campuzano, I. D. G.; Larriba, C.; Bagal, D.; Schnier, P. D., Ion Mobility and Mass Spectrometry Measurements of the Humanized IgGk NIST Monoclonal Antibody. In *State-of-the-Art and Emerging Technologies for Therapeutic Monoclonal Antibody Characterization Volume 3. Defining the Next Generation of Analytical and Biophysical Techniques*, American Chemical Society: 2015; Vol. 1202, pp 75-112.
61. Gozzo, T. A.; Bush, M. F. Quantitatively Differentiating Antibodies Using Charge-State Manipulation, Collisional Activation, and Ion Mobility-Mass Spectrometry. *Anal Chem* **2023**.
62. Shaw, J. B.; Li, W.; Holden, D. D.; Zhang, Y.; Griep-Raming, J.; Fellers, R. T.; Early, B. P.; Thomas, P. M.; Kelleher, N. L.; Brodbelt, J. S. Complete protein characterization using top-down mass spectrometry and ultraviolet photodissociation. *J Am Chem Soc* **2013**, *135* (34), 12646-51.
63. Rush, M. J. P.; Riley, N. M.; Westphall, M. S.; Coon, J. J. Top-Down Characterization of Proteins with Intact Disulfide Bonds Using Activated-Ion Electron Transfer Dissociation. *Anal Chem* **2018**, *90* (15), 8946-8953.
64. Chen, J.; Shiyanov, P.; Zhang, L.; Schlager, J. J.; Green-Church, K. B. Top-down characterization of a native highly intralinked protein: concurrent cleavages of disulfide and protein backbone bonds. *Anal Chem* **2010**, *82* (14), 6079-89.
65. Ganisl, B.; Breuker, K. Does Electron Capture Dissociation Cleave Protein Disulfide Bonds? *ChemistryOpen* **2012**, *1* (6), 260-8.
66. Srzentic, K.; Fornelli, L.; Tsybin, Y. O.; Loo, J. A.; Seckler, H.; Agar, J. N.; Anderson, L. C.; Bai, D. L.; Beck, A.; Brodbelt, J. S.; van der Burgt, Y. E. M.; Chamot-Rooke, J.; Chatterjee, S.; Chen, Y.; Clarke, D. J.; Danis, P. O.; Diedrich, J. K.; D'Ippolito, R. A.; Dupre, M.; Gasilova, N.; Ge, Y.; Goo, Y. A.; Goodlett, D. R.; Greer, S.; Haselmann, K. F.; He, L.; Hendrickson, C. L.; Hinkle, J. D.; Holt, M. V.; Hughes, S.; Hunt, D. F.; Kelleher, N. L.; Kozhinov, A. N.; Lin, Z.; Malosse, C.; Marshall, A. G.; Menin, L.; Millikin, R. J.; Nagornov, K. O.; Nicolardi, S.; Pasa-Tolic, L.; Pengelley, S.; Quebbemann, N. R.; Resemann, A.; Sandoval, W.; Sarin, R.; Schmitt, N. D.; Shabanowitz, J.; Shaw, J. B.; Shortreed, M. R.; Smith, L. M.; Sobott, F.; Suckau, D.; Toby, T.; Weisbrod, C. R.; Wildburger, N. C.; Yates, J. R., 3rd; Yoon, S. H.; Young, N. L.; Zhou, M. Interlaboratory Study for Characterizing Monoclonal Antibodies by Top-Down and Middle-Down Mass Spectrometry. *J Am Soc Mass Spectrom* **2020**, *31* (9), 1783-1802.